RSC Advances

PAPER

View Article Online
View Journal | View Issue

Cite this: *RSC Adv.*, 2023, **13**, 24201

Effect of microplastics on the binding properties of Pb(II) onto dissolved organic matter: insights from fluorescence spectra and FTIR combined with two-dimensional correlation spectroscopy†

Weiqian Liang, ‡* Shuyin Wei,‡ Longxia Lan, Jinfeng Chen, Yingyue Zhou, Jiawei Zhao, Hao Wang, Rui Gao and Feng Zeng

Heavy metal cations are a typical type of inorganic pollutant that has persistent distribution characteristics in aquatic environments and are easily adsorbed on carriers, posing serious threats to ecological safety and human health. Some studies have shown that the coexistence of dissolved organic matter (DOM) and microplastics (MPs) promotes the adsorption of heavy metal cations, but the mechanism of promoting the adsorption process has not been thoroughly studied. In this study, the effect of polystyrene microplastics (PSMPs) on the binding properties of Pb^{2+} onto humic acid (HA) in aquatic environments was investigated by spectral analysis and two-dimensional correlation (2D-COS) analysis. When PSMPs co-existed with HA, the adsorption capacity of Pb^{2+} increased. On the one hand, Pb^{2+} is directly adsorbed on HA through the mechanism of complexation reaction, ion exchange and electrostatic interaction. On the other hand, Pb^{2+} is first adsorbed on PSMPs by electrostatic action and indirectly adsorbed on HA in the form of PSMPs–Pb^{2+} owing to the interaction between HA and PSMPs, which increases the adsorption amount of Pb^{2+} on HA. This study is significant for studying the migration and regression of heavy metal cation contaminants when PSMPs co-exist with DOM in an aqueous environment.

Received 22nd June 2023
Accepted 1st August 2023

DOI: 10.1039/d3ra04189a

rsc.li/rsc-advances

1 Introduction

Heavy metals are of great concern in aquatic environments because of the features of trace quantities and permanence properties in the environment; heavy metals have seriously threatened ecological security and human health.[1,2] For example, copper, lead, nickel, chromium, and mercury may be lethal threats to multiple organisms even at a very low exposure dose.[3,4] Among them, lead (Pb) is one of the most widely used and distributed categories in the environment.[5–7] However, when the blood Pb level of children is above 10 μg dL^{-1}, it can cause irreversible damage to intelligent development.[8] Therefore, it is particularly important to investigate the environmental behavior of heavy metals owing to their accumulation potential and toxicity in sediments and organisms.

Dissolved organic matter (DOM) is ubiquitous in natural waters and is composed of multiple organic components and functional groups.[9–11] Previous studies have revealed that owing to the presence of functional groups, such as hydroxylic, carboxylic and alcohol hydroxylic groups, DOM can interact with metal ions in several ways, including complexation, ion exchange and reduction, which indicates that DOM is believed to have important effects on heavy metal speciation, transport, and bioavailability.[12–14] However, in reality, in environments other than heavy metals and DOM, other inorganic/organic pollutants are also present; inevitable interactions result in more complex environmental behaviors. For example, sediment resuspension in lake water significantly decreases the heavy metal binding affinity of DOM, which might be attributed to binding competition from inorganic colloids.[15] Clay minerals and iron-bearing minerals in rocks significantly affect the binding characteristics of colloidal organic matter (COM), which are important parts of DOM, and metal ions under water–rock interaction.[16]

Among the numerous coexisting pollutants, microplastics (MPs) undoubtedly deserve more attention because of their inherent harmfulness and interactions with others, as well as a potential cluster for contaminates.[17,18] MPs could be stable in aquatic environments for a long time owing to special characteristics (light weight, small particle sizes, strong hydrophobicity, variable density and large specific surface area).[19–21] Moreover, owing to these unique properties, MPs can sorb

School of Chemistry, Sun Yat-sen University, Guangzhou, 510275, China. E-mail: liangwq3@mail2.sysu.edu.cn; qian378378@163.com; Tel: +86-20-84114133

† Electronic supplementary information (ESI) available. See DOI: https://doi.org/10.1039/d3ra04189a

‡ Weiqian Liang and Shuyin Wei contribute equally to the article.

numerous pollutants (*e.g.*, heavy metals[22–24] and organic pollutants[25,26]) from the surrounding aquatic environments and act as carriers owing to their long-term transport in aquatic ecosystems, thereby resulting in even more significant hazards to organisms.[27] MPs in actual environments experience aging under the influence of various factors, such as light and microorganisms, which may change the morphology and structure of MPs, thus affecting their environmental behaviors and interactions with pollutants.[28–30] According to previous studies, the occurrence of MPs in soil increased the adsorption capacity for 17β-estradiol (E2), and the additional amount and aging of MPs enhanced the promotion effect.[26] However, the addition of MPs significantly decreased the overall sorption of diazepam on the soil at 10% and increased the sorption of phenanthrene at 1%, while the effects were negligible at other addition rates.[31] Although there have been many reports on the effect of MPs on adsorption, no systematic study exists on how MPs affect the binding characteristics of DOM with heavy metals.

In this study, humic acid (HA), a representative dissolved organic matter (DOM), was selected for the reactions. Moreover, polystyrene microplastics (PSMPs) were selected as representative MPs to explore the effect of MP occurrence on the adsorption of Pb^{2+} in HA by batch experiments. 3D-excitation emission matrix (3D-EEM) fluorescence spectroscopy, synchronous fluorescence (SF) spectroscopy, and Fourier transform infrared (FTIR) spectroscopy analyses were used to track the structural changes in HA in its interaction process with Pb^{2+}. Moreover, two-dimensional correlation spectroscopy (2D-COS) analysis[32–36] was used to provide detailed information on the binding interactions between Pb^{2+} and HA under the influence of PSMPs by enhancing the spectral resolution and integrating complementary information, which solved the problem of spectral peak overlap. This study provides insight into the mechanism of Pb^{2+} adsorption in the coexistence of PSMPs and HA. The results of this study are significant for understanding the environmental behavior of heavy metal ions in aqueous environments.

2 Materials and methods

2.1. Reagents and materials

PSMPs and HA were purchased from Sigma-Aldrich (St. Louis, MO, USA). Lead nitrate ($Pb(NO_3)_2$), nitric acid (HNO_3) and sodium hydroxide (NaOH) were obtained from Guangzhou Chemical Reagent Co., Ltd. (Guangzhou, China). All chemicals were of A.R. grade.

2.2. Aging of PSMPs and characteristic analysis

Aging experiments of PSMPs were performed by exposing them approximately in a simulated environment in a UV-lamp weathering test chamber (γ_{max} = 254 nm). In detail, the PSMPs were washed with deionized water and dried as pretreatment. Subsequently, the PSMPs were aged in the air, and the conditions of photo-aging were described as follows: temperature = 60 °C; humidity = 70%; and light irradiance = 1200 W m^{-2}. The UV radiation time of PSMPs in this experiment ranged from 1 day to 7 days. PSMPs with an aging time of 5 days were selected as the model PSMPs.

To better explore the changes in surface structure, specific surface area and functional groups of MPs in the UV aging process, PSMPs at a specific time point were characterized in the experiment. The surface morphologies of PSMPs subjected to different ultraviolet radiation times were analyzed by scanning electron microscopy (SEM, Hitachi S-4800) at 5.0 kV. To calculate the specific surface area of the experimental MP samples, a nitrogen adsorption–desorption analytical method was adopted to obtain accurate data using an ASAP2020 instrument (Micromeritics, USA) at 77 K. Surface charge changes in PSMPs during the aging process were measured by applying a Malvern Zetasizer instrument (Nano ZS, UK). Fourier transform infrared spectroscopy (FT-IR, Nicolet iS50, Thermo Electron Corp., USA) was employed to determine the changes in the surface functional groups of the pristine and aged PSMPs.

2.3. Adsorption experiment

In the experiment, HA solutions with different concentrations were obtained by dilution of the stock solution (250 mg C per L). Pb^{2+} stock solution (500 mg L^{-1}) was obtained by dissolving $Pb(NO_3)_2$ in distilled water, and the pH was adjusted to 5.0 with 0.10 mol L^{-1} HNO_3 or 0.10 mol L^{-1} NaOH.

They were conducted in a conical flask with PSMPs as well as 20 mL of a mixed solution of HA and Pb^{2+}, where the concentration of HA was maintained at 10 mg C per L and the concentration of PSMPs was adjusted to different levels (0, 0.50, 1.0, 2.0, 5.0, 10 and 100 mg C per L) based on previous relevant studies. For the sorption isotherms, the initial concentrations of Pb^{2+} were 0, 0.50, 1.0, 2.0, 5.0, 10 and 20 mg L^{-1}. The conical flasks were shaken in a shaker under a constant temperature of 298 K at 150 rpm. After reaching adsorption equilibrium, these mixed solutions were filtered through 0.45 μm aqueous membrane filters. A 5 mL filtrate of each sample was used for the fluorescence spectroscopy analysis. The rest of the filtrate was freeze-dried for further FTIR spectroscopy analysis. All samples were subjected to three parallel experiments.

2.4. Procedures and instrumental parameters of measurements

The 3D-EEM spectrum of the filtrate solutions was determined by employing a Cary Eclipse spectrometer (Shimadzu Co., Japan). The parameters of fluorescence measurement were set as follows: emission (Em) wavelengths were in the range of 300–600 nm, excitation (Ex) wavelengths were in the range of 220–550 nm, slit width was 5 nm, scan rate = 2400 nm min^{-1}, and voltage = 600 V. Ultrapure Milli-Q water was used as a blank.

The SF spectra of the filtrate solutions were obtained by averaging the spectrums of the three scans using a luminescence spectrometer (Shimadzu Co., Japan). The Ex and Em slits were both set at 5 nm, and the excitation wavelength range was 300–600 nm with 1 nm increments. The scan rate was 2000 nm min^{-1}, and the offset $\Delta\lambda$ ($\lambda_{Em} - \lambda_{Ex}$) was set constant at

80 nm to provide moderate fluorescence intensity and better resolution, as described in a previous study.

The powder was obtained by freeze-drying the filtrate solutions, and the structural and chemical characteristics were analyzed using FTIR spectra. FTIR spectra from 3600 to 400 cm^{-1} were generated using a PerkinElmer Spectrum One FTIR spectrometer (PerkinElmer, USA).

3 Results and discussion

3.1. Characterizations of PSMPs and HA

The SEM images of aged PSMP particles indicate that cracks and pits were formed during the aging process (Fig. 1a). Cracks and pits gradually increased on the surfaces of the microplastics as the aging time increased. The BET data (Table S1†) indicate that aging increases the surface areas of the PSMPs significantly (surface area of aged PSMP 13.6–54.8 $m^2\ g^{-1}$ compared to 3.68 $m^2\ g^{-1}$ for pristine PSMP). The zeta potentials of the original and aged PSMPs under the condition of different pH values are shown in Fig. S1.† It could be found that both the zeta potentials of PSMPs were negatively charged, and the $|\zeta|$ of aged PSMPs clearly increased with the aging time, which could be explained by the carbonyl group formed on the surface of the PSMPs after the photo-oxidation process.

Fig. 1b and S2† show that the FT-IR absorption peaks of PSMPs before and after aging were basically similar, with only some absorption peaks differing slightly. The peaks at 3400–3600 cm^{-1} related to the O–H stretching vibration and characteristic peaks of C=O at 1731 cm^{-1} can be observed in the FTIR spectra of aged PSMPs, but they cannot be found in that of virgin PSMPs. These results are the same as those of previous studies in which the aging process increases the oxygen-containing functional groups of PSMPs.[24,30]

The characteristics of HA (Fig. S3†) have been described in previous studies.[37] In the FTIR of HA, a significant peak at 3343 cm^{-1} represents the O–H stretching of carboxylic acids, phenols, or alcohols; 1620, 1340, and 1573 cm^{-1} represent the carboxylate C=O stretching vibration, the C–O stretching vibration of esters, ethers, or phenols, and the C=C stretching vibration of aromatic rings, respectively. These results indicate that HA is rich in oxygen-containing functional groups and aromatic rings.[38,39]

3.2. Effect of PSMPs on the fluorescence spectroscopic responses of HA to Pb^{2+} binding

Fig. S3a† shows that three peaks were observed in HA: Peak A (Ex/Em = 310/480 nm) represents fulvic-like fractions, and Peak B (Ex/Em = 465/525 nm) and Peak C (Ex/Em = 385/490 nm) represent humic-like fractions.[40,41] In the HA–Pb^{2+} system (Fig. S4†), with the addition of Pb^{2+}, Peaks B and C gradually disappeared, and the excitation wavelength of Peak A showed an obvious blue shift, indicating a decreasing content of aromaticity and polycondensation of humic substances.[37] In the HA–PSMPs system (Fig. S5†), with the addition of PSMPs, Peaks A, B and C all have only a small reduction. In the HA–PSMPs–Pb^{2+} system (Fig. S6†), Peaks A, B and C reduced rapidly with increasing concentrations of Pb when the PSMP concentration was fixed, and the quenching of HA was stronger than that in the binary system.

The changes in synchronous fluorescence spectra of HA with Pb^{2+} binding in the presence and absence of PSMPs are displayed in Fig. 2a–c. According to the literature,[34,40] three fluorescence regions corresponding to the wavelength ranges of 280–360 nm, 360–440 nm, and 440–600 nm could be roughly assigned to protein-like, fulvic-like, and humic-like fluorophore fractions, respectively. It was observed that there were two strong fluorescence peaks at Em = 430 nm and Em = 490 nm in the samples, which were representative of the fulvic-like and humic-like fractions in HA, respectively. There is a possible difference in the complexation of HA components with Pb^{2+} or PSMPs. Therefore, the modified Stern–Volmer equation was used to calculate the complexation ability of different fractions in HA with Pb^{2+} or PSMPs (Fig. 2d–f), and the modeling results are presented in Table 1.

In the HA–Pb^{2+} system, specifically, strong quenching effects were observed in both humic-like and fulvic-like components with the addition of Pb^{2+}. The conditional stability constants log K_m and the fractions of the initial fluorescence f of the fulvic-

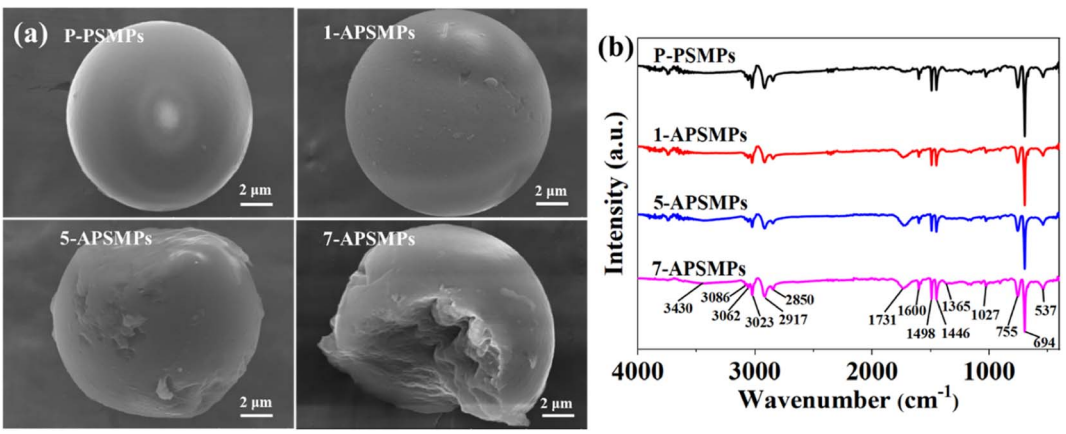

Fig. 1 SEM (a) and FTIR (b) of pristine PSMPs and aged PSMPs.

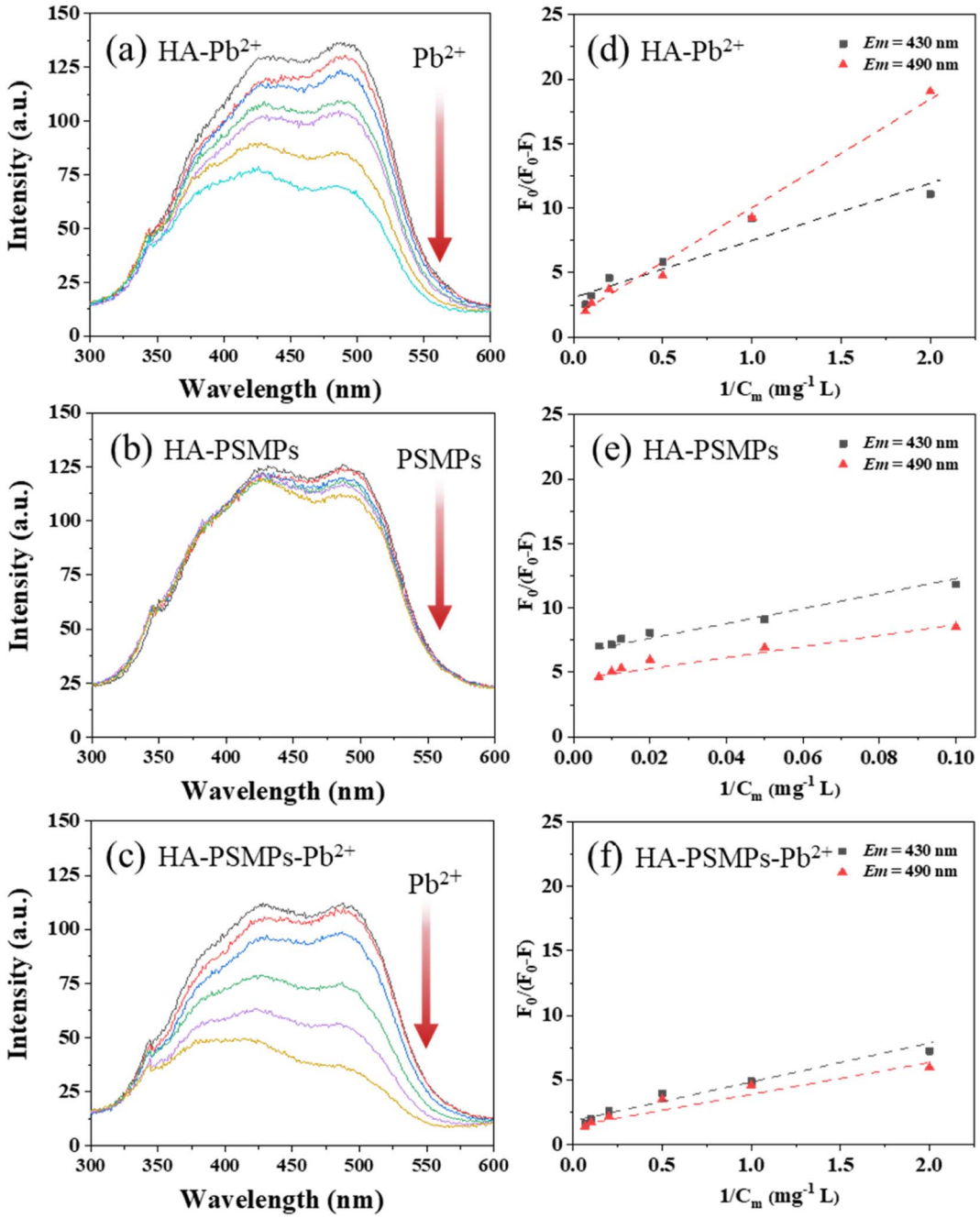

Fig. 2 SF of HA in HA–Pb^{2+} system (a), HA–PSMPs system (b), and HA–PSMPs–Pb^{2+} system (c); variation of SF of HA fitted by modified Stern–Volmer equation model in the HA–Pb^{2+} system (d), HA–PSMPs system (e), and HA–PSMPs–Pb^{2+} system (f).

like fractions were 3.33 and 0.305, respectively, which were slightly lower than those of 3.38 and 0.734 for the humic-like fractions, suggesting that these two components were both involved in Pb^{2+} binding to HA.

However, in the HA–PSMP system, less significant quenching effects were observed in the fulvic-like fraction of HA with the addition of PSMPs compared to the humic-like fraction, revealing much stronger adsorption of humic-like components on PSMPs. These results are the same as those of previous studies[42] because of the high content of phenolic and aromatic carboxylic groups of the humic-like fraction, which could bind PSMPs through π–π interactions and hydrophobic interactions.

In the HA–PSMP–Pb^{2+} system, the decrease in the relative intensity of humic-like fractions was more significant than that of the fulvic-like fractions after adsorption. Compared to the HA without PSMPs, the $\log K_m$ and f values for HA with PSMPs were higher. In addition, an increase in PSMP dose led to higher values of $\log K_m$ and f values. These results suggest that PSMPs and Pb^{2+} both could bind to the humic-like fraction of HA.

Table 1 Modified Stern–Volmer equation model parameters

	Peak (Em = 430 nm)			Peak (Em = 490 nm)		
System	f	Log K_m	R	f	Log K_m	R
HA–Pb^{2+}	0.305	3.88	0.915	0.734	3.33	0.990
HA–PSMPs	0.147	3.14	0.989	0.209	3.14	0.962
HA–PSMPs–Pb^{2+} (HA : PSMPs)						
1 : 0.01	0.323	3.76	0.977	0.629	3.77	0.937
1 : 0.1	0.330	3.80	0.964	0.633	3.83	0.969
1 : 0.5	0.331	3.83	0.965	0.638	3.94	0.929
1 : 1	0.340	3.84	0.965	0.657	3.97	0.900
1 : 5	0.346	3.88	0.947	0.672	4.02	0.935
1 : 10	0.370	3.89	0.966	0.694	4.09	0.928

Overall, compared with the HA without PSMPs added, the adsorption capacity of HA to Pb^{2+} was significantly increased by adding PSMPs, which was the same as the results of previous studies.[37] Because previous studies[37] found a relatively high adsorption capacity of PSMPs for Pb^{2+}, the addition of PSMPs to HA contributes to a "superimposed effect", which may be part of the reason for the enhancement in HA adsorption. In addition, the binding of PSMPs to HA brings in more adsorption sites, resulting in enhanced hydrogen bonding and π–π interactions between HA and Pb^{2+}.

3.3. Binding characterized by 2D-SFS-COS

To further investigate the binding characteristics, the 2D-COS spectrum generated from the SF of HA–Pb^{2+}, HA–PSMPs and

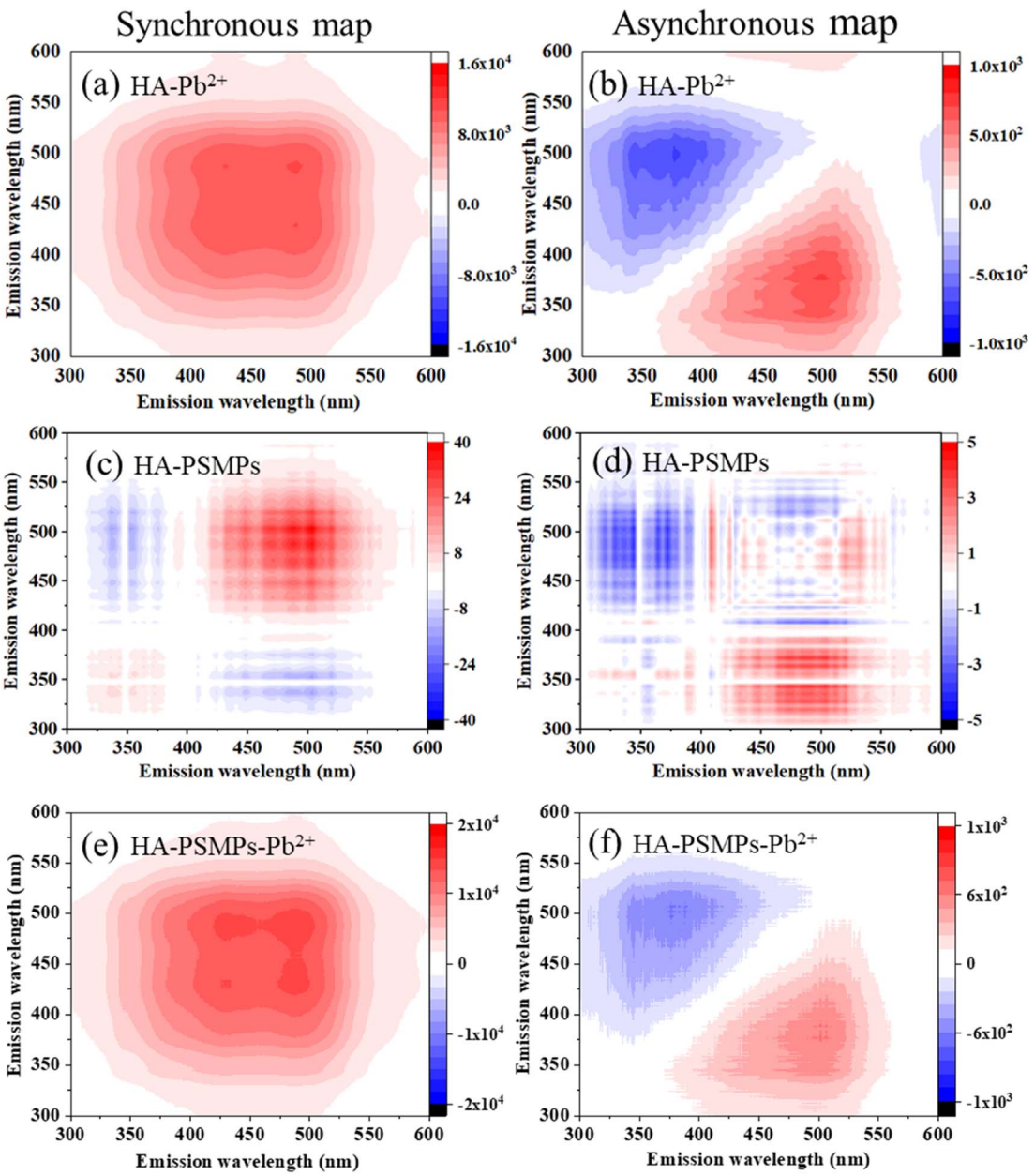

Fig. 3 2D-SF-COS diagram of HA in the HA–Pb^{2+} system (a and b), HA–PSMPs system (c and d), and HA–PSMPs–Pb^{2+} system (e and f).

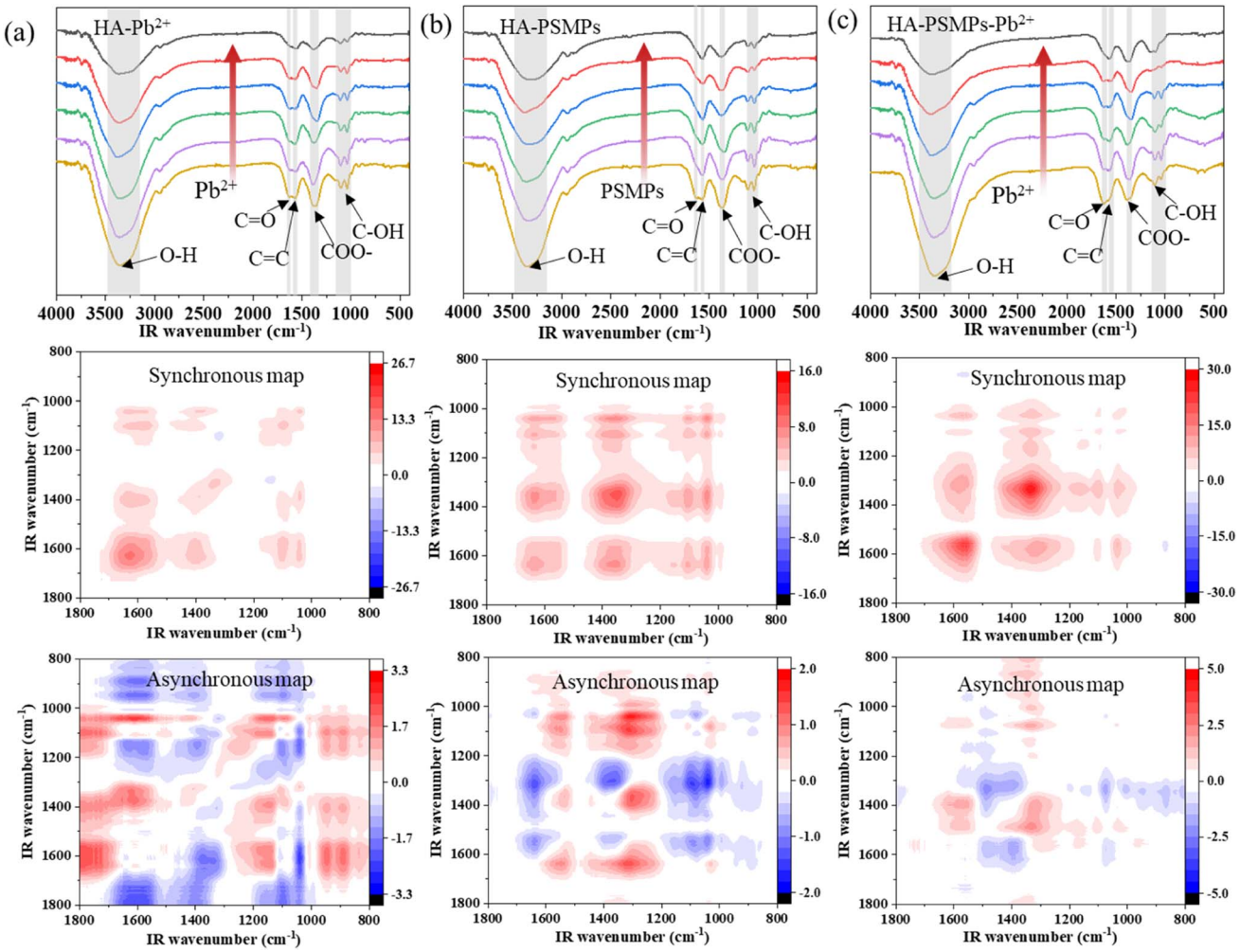

Fig. 4 FTIR and 2D-FTIR-COS of HA in the HA–Pb^{2+} system (a), HA–PSMPs system (b), and HA–PSMPs–Pb^{2+} system (c).

HA–PSMPs–Pb^{2+} was illustrated in Fig. 3. The synchronous map of HA–Pb^{2+} gave two positive auto-peaks at 430 and 490 nm with the peak intensity of corr. = 9304 (430 nm) ≈ corr. = 9060 (490 nm), which indicated that Pb^{2+} resulted in different electronic structural changes in the two fluorescence fractions through forming complexes with HA. In the asynchronous map, four positive cross-peaks (498/378, 498/388, 498/412 and 590/412 nm) were identified in the upper-left corner. According to Noda's rules, the sequential order for the peak change was 498 → 590 → 388 → 378 → 412 nm, indicating that Pb^{2+} bound to HA in the following order: humic-like fractions → fulvic-like fractions, which is consistent with the modified Stern–Volmer equation modeling results.

Five positive cross-peaks can be found at 445, 472, 490, 500 and 520 nm of the HA–PSMP system in the synchronous map. It can be observed from comparing the peak intensities that the humic-like fractions are more susceptible to changes in the concentration of PSMPs. This may be due to the high content of phenolic and aromatic carboxylic groups of the humic-like fraction, which could bind PSMPs through π–π interactions and hydrophobic interactions. Based on the asynchronous maps, 410 → 502 → 490 → 370 → 410 → 390 → 364 nm showed that the fluorescent structure variation sequence was humic-like fraction → fulvic-like fraction.

In the HA–PSMP–Pb^{2+} system, two auto-correlation peaks centered at 430 and 490 nm with a peak intensity of 490 nm ≈ 430 nm were found in the synchronous maps, indicating that the sensitivities of the external perturbation of humic-like fractions and fulvic-like fractions were similar. The intensities of the two autocorrelation peaks of HA in the HA–PSMP–Pb^{2+} system were much higher than those in the HA–PSMP system but slightly higher than those in the HA–Pb^{2+} system. These results suggest that the binding capacity of the components of HA increased in the presence of PSMPs. In the asynchronous maps, the fluorescent structure variation sequences were all humic-like fractions → fulvic-like fractions although the spot positions of the cross-peaks were different.

Overall, the sequential order for the binding affinity of Pb^{2+} onto each fraction of HA did not change significantly in the presence or absence of PSMPs. However, the binding sites for the same fluorescence fraction within HA differed among the different adsorption systems.[43] Thus, even in the same

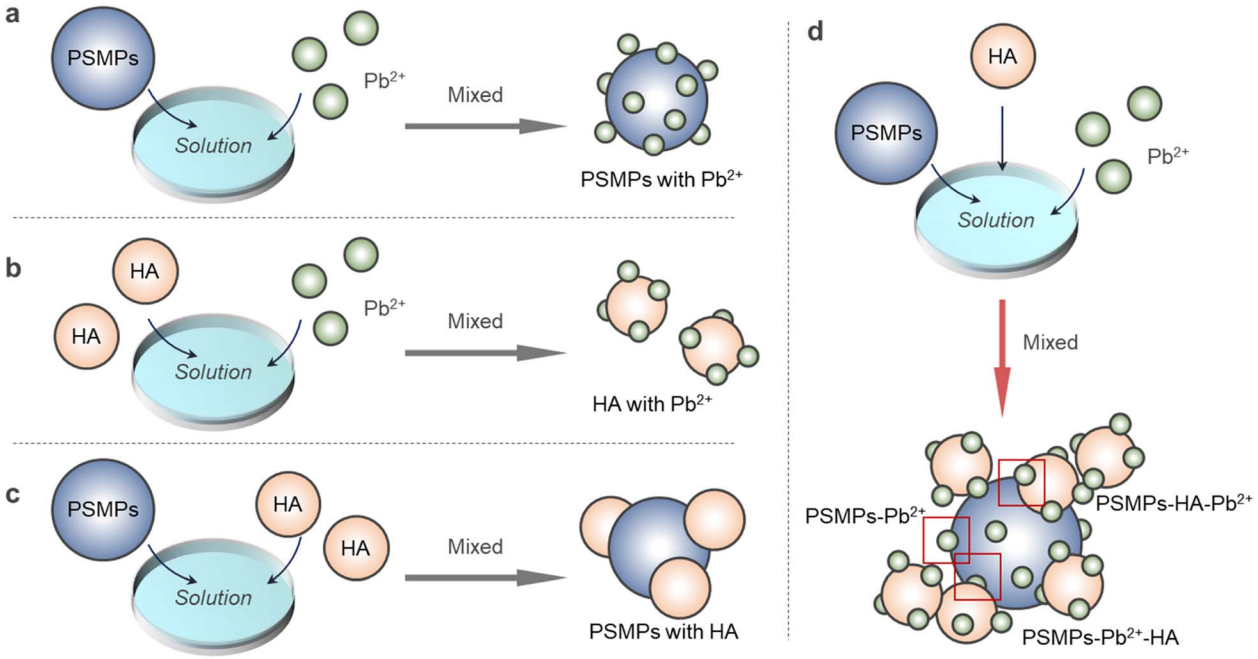

Fig. 5 Diagram of binding mechanism in different systems.

fluorescent component of HA, the binding sites might be non-uniformly distributed,[44] *i.e.*, the binding affinities within the same fluorescent component were different.

3.4. Binding characterized by 2D-FTIR-COS

To clarify the dominant functional groups of HA participating in binding, FTIR spectroscopy for the complexation of HA with Pb or PSMPs was performed (Fig. 4).

In HA–Pb^{2+} system (Fig. 4c), six auto-correlation peaks were observed in the synchronous map: 3343 cm^{-1} (corr. = 111) > 1620 cm^{-1} (corr. = 8.32) > 1340 cm^{-1} (corr. = 5.35) > 1573 cm^{-1} (corr. = 4.01) ≈ 1041 cm^{-1} (corr. = 3.99) ≈ 1103 cm^{-1} (corr. = 3.80). The peak at 3343 cm^{-1} deceased the most with the increase in Pb^{2+} concentration, which represents the O–H stretching of carboxylic acids, phenols or alcohols, followed by FTIR band intensity attenuation at 1620, 1340 and 1573 cm^{-1}, which represent the stretching vibration of carboxyl C=O, the C–O stretching of esters, ethers or phenols and the C=C stretching vibration of aromatic rings, respectively. In the asynchronous map, there are positive and negative cross peaks. According to the sequential order rules, the sequential order for the peak change was 3343 → 1620 → 1340 →1041 → 1103 → 1573 cm^{-1}, indicating that the structural change in HA upon Pb^{2+} binding followed the order of carboxylic acids O–H → carboxyl C=O → esters, ethers or phenols C–O → alcohol C–O → alkene C–H → aromatic rings C=C. These results indicate that carboxyl and phenolic hydroxyl groups are the main binding sites during Pb^{2+} binding by HA, which means that they depend mainly on acidity and aromaticity,[37] in agreement with the results of the fluorescence spectroscopy analysis.

In the HA–PSMP system (Fig. 4b), the effects of pristine and aged PSMPs on the FTIR of HA were similar; six auto-correlation peaks centered at 3343, 1620, 1573, 1340, 1103, and 1040 cm^{-1} were observed in the synchronous map. The results suggest that the sensitivity of each group in HA to PSMP external perturbation followed the order of carboxylic acids O–H > esters, ethers or phenols C–O > carboxyl C=O > aromatic rings C=C > alcohol C–O > alkene C–H. In the asynchronous map, the sequential order for the peak change was 1620 → 1573 → 1340 → 3343 cm^{-1}, which suggests that the unsaturated bonds and aromatic compounds in HA preferentially bonded to PSMPs owing to the increase in oxygen-containing functional groups in PSMPs after aging.[45,46]

The 2D-FTIR-COS of four HA–PSMP–Pb^{2+} systems is shown in Fig. 4c. The auto-peaks mainly existing at 3343, 1620, 1573, 1340, 1103, and 1040 cm^{-1} in the synchronous map were very similar to the results of HA–Pb^{2+} system, which suggests a similar complexation mechanism between Pb^{2+} and HA when PSMPs were present and absent. The most susceptive functional group of HA was the peaks at 3343 cm^{-1}, followed by 1340, 1620 and 1573 cm^{-1}. Thus, carboxylic acid and aromatic rings of HA may be the components with the strongest complexing ability in all three systems. However, differences were observed in the susceptibility and binding sequences of the corresponding spectral region. Compared with the HA–Pb^{2+} system and the HA–PSMP system, the intensity of the peaks at the same positions in the HA–PSMP–Pb^{2+} system increased, which means that the binding ability of the functional group of HA was stronger in the ternary system. By analyzing the signs of cross-peaks in synchronous and asynchronous maps, the sequential order for peak change was 1620 → 1573 → 1340 → 3343 cm^{-1}, suggesting that the rank for the bonding of functional groups in HA was carboxylic acids O–H → carboxyl C=O → aromatic rings C=C → esters, ethers or phenols C–O. In addition, as shown in

Fig. 2, the amount of PSMPs added also affects the binding degree and binding order of the functional groups of HA.

4 Conclusions

The influence mechanism of PSMPs on the adsorption of Pb^{2+} by HA was analyzed by spectral analysis. The results are shown in Fig. 5. When HA adsorbed Pb^{2+}, it was mainly the carboxyl and hydroxyl groups of HA that bonded with Pb^{2+}. In the binding process of HA and PSMPs, humic-like binding is mainly involved, and the binding ability is higher than that of fulvic-like binding. Because of the high content of the aromatic ring in HA's humic-like, PSMPs are bound by π–π conjugation and hydrophobic interaction. When PSMPs co-existed with HA, the adsorption capacity of Pb^{2+} onto HA increased. On the one hand, Pb^{2+} is directly adsorbed on HA through the mechanism of complexation reaction, ion exchange and electrostatic interaction. On the other hand, Pb^{2+} is first adsorbed on PSMPs by electrostatic action and indirectly adsorbed on HA in the form of PSMPs–Pb^{2+} due to the interaction between HA and PSMPs, which increases the adsorption amount of Pb^{2+} on HA. This study is significant for investigating the migration and regression of heavy metal cation contaminants when DOMs and PSMPs coexist in aqueous environments.

Consent to participate

All authors have given consent to their contribution.

Consent for publication

All authors have agreed with the content and all have given explicit consent to publish.

Author contributions

Weiqian Liang, investigation and original draft preparation; Shuyin Wei, data analysis; Longxia Lan, data analysis; Jinfeng Chen, data analysis; Yingyue Zhou, sample collection; Jiawei Zhao, sample collection; Hao Wang, sample collection; Rui Gao, sample collection; Feng Zeng, supervisor, funding support, writing review.

Conflicts of interest

The authors declare there is no conflicts of interest regarding the publication of this paper.

Acknowledgements

This work was supported by the Natural Science Foundation of China (No. 41877462).

References

1 J. Swidwa-Urbanska and J. Batlle-Sales, Data quality oriented procedure, for detailed mapping of heavy metals in urban topsoil as an approach to human health risk assessment, *J. Environ. Manage.*, 2021, **295**, 113019.
2 J. Zhao, E. Wu, B. Zhang, *et al.*, Pollution characteristics and ecological risks associated with heavy metals in the Fuyang river system in North China, *Environ. Pollut.*, 2021, **281**, 116994.
3 M. A. Hossen, A. I. H. Chowdhury, M. R. A. Mullick, *et al.*, Heavy metal pollution status and health risk assessment vicinity to Barapukuria coal mine area of Bangladesh, *Environ. Nanotechnol. Monit. Manag.*, 2021, **16**, 100469.
4 C. Yan, Z. Qu, J. Wang, *et al.*, Microalgal bioremediation of heavy metal pollution in water: recent advances, challenges, and prospects, *Chemosphere*, 2022, **286**(pt 3), 131870.
5 S. Liu, J. Huang, W. Zhang, *et al.*, Investigation of the adsorption behavior of Pb(II) onto natural-aged microplastics as affected by salt ions, *J. Hazard. Mater.*, 2022, **431**, 128643.
6 A. Turner, L. Holmes, R. C. Thompson, *et al.*, Metals and marine microplastics: adsorption from the environment versus addition during manufacture, exemplified with lead, *Water Res.*, 2020, **173**, 115577.
7 T. B. Nguyen, T. B. Ho, C. P. Huang, *et al.*, Adsorption of lead(II) onto PE microplastics as a function of particle size: influencing factors and adsorption mechanism, *Chemosphere*, 2022, **304**, 135276.
8 L. Hu, Y. Zhao and H. Xu, Trojan horse in the intestine: a review on the biotoxicity of microplastics combined environmental contaminants, *J. Hazard. Mater.*, 2022, **439**, 129652.
9 H. Dai, T. Sun, T. Han, *et al.*, Interactions between cerium dioxide nanoparticles and humic acid: influence of light intensities and molecular weight fractions, *Environ. Res.*, 2021, **195**, 110861.
10 J. Lv, Y. Miao, Z. Huang, *et al.*, Facet-Mediated Adsorption and Molecular Fractionation of Humic Substances on Hematite Surfaces, *Environ. Sci. Technol.*, 2018, **52**(20), 11660–11669.
11 T. Li, F. Song, J. Zhang, *et al.*, Experimental and modeling study of proton and copper binding properties onto fulvic acid fractions using spectroscopic techniques combined with two-dimensional correlation analysis, *Environ. Pollut.*, 2020, **256**, 113465.
12 X. J. Guo, X. S. He, C. W. Li, *et al.*, The binding properties of copper and lead onto compost-derived DOM using Fourier-transform infrared, UV-vis and fluorescence spectra combined with two-dimensional correlation analysis, *J. Hazard. Mater.*, 2019, **365**, 457–466.
13 Y. Ding, M. Liu, S. Peng, *et al.*, Binding characteristics of heavy metals to humic acid before and after fractionation by ferrihydrite, *Chemosphere*, 2019, **226**, 140–148.
14 J. Wang, C. Lü, J. He, *et al.*, Binding characteristics of Pb2+ to natural fulvic acid extracted from the sediments in Lake Wuliangsuhai, Inner Mongolia plateau, P. R. China, *Environ. Earth Sci.*, 2016, **75**(9), 768.
15 T. Bao, P. Wang, B. Hu, *et al.*, Investigation on the effects of sediment resuspension on the binding of colloidal organic

matter to copper using fluorescence techniques, *Chemosphere*, 2019, **236**, 124312.

16 K. Zhang, J. Gao, D. Men, *et al.*, Insight into the heavy metal binding properties of dissolved organic matter in mine water affected by water-rock interaction of coal seam goaf, *Chemosphere*, 2021, **265**, 129134.

17 F. Zhang, G. Peng, P. Xu, *et al.*, Ecological risk assessment of marine microplastics using the analytic hierarchy process: a case study in the Yangtze River Estuary and adjacent marine areas, *J. Hazard. Mater.*, 2022, **425**, 127960.

18 M. Enfrin, R. Myszka and F. Giustozzi, Paving roads with recycled plastics: microplastic pollution or eco-friendly solution?, *J. Hazard. Mater.*, 2022, **437**, 129334.

19 Y. Sun, L. Cao, Y. Wang, *et al.*, Sources and distribution of microplastics in the east China sea under a three-dimensional numerical modelling, *Environ. Pollut.*, 2022, **311**, 119910.

20 Y. Ding, X. Zou, H. Chen, *et al.*, Distribution pattern and influencing factors for the microplastics in continental shelf, slope, and deep-sea surface sediments from the South China Sea, *Environ. Pollut.*, 2022, **309**, 119824.

21 A. Sholokhova, G. Denafas and V. Mykhaylenko, Microplastics generation and concentration during mechanical-biological treatment of mixed municipal solid waste, *Environ. Res.*, 2022, **214**(pt 1), 113815.

22 W. He, S. Zheng, X. Chen, *et al.*, Alkaline aging significantly affects Mn(II) adsorption capacity of polypropylene microplastics in water environments: critical roles of natural organic matter and colloidal particles, *J. Hazard. Mater.*, 2022, **438**, 129568.

23 Y. Li, Y. Zhang, F. Su, *et al.*, Adsorption behaviour of microplastics on the heavy metal Cr(VI) before and after ageing, *Chemosphere*, 2022, **302**, 134865.

24 Z. Zhou, Y. Sun, Y. Wang, *et al.*, Adsorption behavior of Cu(II) and Cr(VI) on aged microplastics in antibiotics-heavy metals coexisting system, *Chemosphere*, 2022, **291**(pt 1), 132794.

25 F. a. O. Udenby, H. Almuhtaram, M. J. Mckie, *et al.*, Adsorption of fluoranthene and phenanthrene by virgin and weathered polyethylene microplastics in freshwaters, *Chemosphere*, 2022, **307**(pt 1), 135585.

26 B. Hu, Y. Li, L. Jiang, *et al.*, Influence of microplastics occurrence on the adsorption of 17beta-estradiol in soil, *J. Hazard. Mater.*, 2020, **400**, 123325.

27 D. D. Pramanik, S. Lei, P. Kay, *et al.*, Investigating on the toxicity and bio-magnification potential of synthetic glitters on Artemia salina, *Mar. Pollut. Bull.*, 2023, **190**, 114828.

28 X. Liu, P. Sun, G. Qu, *et al.*, Insight into the characteristics and sorption behaviors of aged polystyrene microplastics through three type of accelerated oxidation processes, *J. Hazard. Mater.*, 2021, **407**, 124836.

29 H. Luo, Y. Zhao, Y. Li, *et al.*, Aging of microplastics affects their surface properties, thermal decomposition, additives leaching and interactions in simulated fluids, *Sci. Total Environ.*, 2020, **714**, 136862.

30 R. Mao, M. Lang, X. Yu, *et al.*, Aging mechanism of microplastics with UV irradiation and its effects on the adsorption of heavy metals, *J. Hazard. Mater.*, 2020, **393**, 122515.

31 B. Xu, D. Huang, F. Liu, *et al.*, Contrasting effects of microplastics on sorption of diazepam and phenanthrene in soil, *J. Hazard. Mater.*, 2021, **406**, 124312.

32 Y. Park, S. Jin, I. Noda, *et al.*, Emerging developments in two-dimensional correlation spectroscopy (2D-COS), *J. Mol. Struct.*, 2020, **1217**, 128405.

33 Y. K. Lee, S. Hong and J. Hur, Copper-binding properties of microplastic-derived dissolved organic matter revealed by fluorescence spectroscopy and two-dimensional correlation spectroscopy, *Water Res.*, 2021, **190**, 116775.

34 H. Luo, Q. Cheng, D. He, *et al.*, Binding of methylmercury to humic acids (HA): influence of solar radiation and sulfide addition reaction of HA, *Sci. Total Environ.*, 2022, **827**, 154356.

35 Z. L. Liao, Z. C. Zhao, J. C. Zhu, *et al.*, Complexing characteristics between Cu(II) ions and dissolved organic matter in combined sewer overflows: implications for the removal of heavy metals by enhanced coagulation, *Chemosphere*, 2021, **265**, 129023.

36 D. Liu, H. Gao, H. Yu, *et al.*, Applying EEM-PARAFAC combined with moving-window 2DCOS and structural equation modeling to characterize binding properties of Cu (II) with DOM from different sources in an urbanized river, *Water Res.*, 2022, **227**, 119317.

37 X. Lu, F. Zeng, S. Wei, *et al.*, Effects of humic acid on Pb(2+) adsorption onto polystyrene microplastics from spectroscopic analysis and site energy distribution analysis, *Sci. Rep.*, 2022, **12**(1), 8932.

38 J. Kovacik, M. Bujdos and P. Babula, Impact of humic acid on the accumulation of metals by microalgae, *Environ. Sci. Pollut. Res. Int.*, 2018, **25**(11), 10792–10798.

39 A. G. Prado, J. D. Torres, P. C. Martins, *et al.*, Studies on copper(II)- and zinc(II)-mixed ligand complexes of humic acid, *J. Hazard. Mater.*, 2006, **136**(3), 585–588.

40 H. Luo, Q. Cheng, D. He, *et al.*, Effects of photo-irradiation on mercury binding to dissolved organic matter: insights from FT-IR and synchronous fluorescence two-dimensional correlation spectroscopy, *Chemosphere*, 2022, **287**(pt 1), 132027.

41 R. Gao, K. Cui, W. Liang, *et al.*, Molecular weight-dependent adsorption heterogeneities of humic acid on microplastics in aquatic environments: further insights from fluorescence spectra combined with two-dimensional correlation spectroscopy and site energy distribution analysis, *J. Environ. Chem. Eng.*, 2022, **10**(6), 108948.

42 A. Abdurahman, K. Cui, J. Wu, *et al.*, Adsorption of dissolved organic matter (DOM) on polystyrene microplastics in aquatic environments: kinetic, isotherm and site energy distribution analysis, *Ecotoxicol. Environ. Saf.*, 2020, **198**, 110658.

43 X. Zhang, X. Cai, Z. Wang, *et al.*, Insight into metal binding properties of biochar-derived DOM using EEM-PARAFAC and differential absorption spectra combined with two-dimensional correlation spectroscopy, *Environ. Sci. Pollut. Res. Int.*, 2021, **28**(11), 13375–13393.

44 N. Habibul and W. Chen, Structural response of humic acid upon binding with lead: a spectroscopic insight, *Sci. Total Environ.*, 2018, **643**, 479–485.

45 R. Gao, K. Cui, W. Liang, *et al.*, Molecular weight-dependent adsorption heterogeneities of humic acid on microplastics in aquatic environments: further insights from fluorescence spectra combined with two-dimensional correlation spectroscopy and site energy distribution analysis, *J. Environ. Chem. Eng.*, 2022, **10**(6), 108948.

46 A. Abdurahman, K. Cui, J. Wu, *et al.*, Adsorption of dissolved organic matter (DOM) on polystyrene microplastics in aquatic environments: kinetic, isotherm and site energy distribution analysis, *Ecotoxicol. Environ. Saf.*, 2020, **198**, 110658.